Final Report – ERC_HU_15 117680

Exploration of novel genome-maintaining mechanisms using advanced imaging technologies

Mihály Kovács *Department of Biochemistry, Eötvös Loránd University*

Overall goal of project

The genomic DNA of all living organisms is constantly exposed to damage. The most dangerous DNA lesions are double-strand breaks (DSBs), which can result in genomic instability and cancer. Error-free repair of DSBs can be achieved via homologous recombination (HR). Besides DSB repair, HR is also used to generate genetic diversity and ensure proper chromosome segregation during meiosis. RecQ-family DNA helicases are central engines and/or regulators of HR. These enzymes can unwind and restructure DNA molecules. Their deficiencies cause excessive recombination, high cancer predisposition and accelerated ageing.

Earlier we found that RecQ helicases, including human Bloom's syndrome helicase (BLM, a RecQ family member) perform versatile complex activities to process HR-intermediate DNA structures. In the reported project, we set out to

- explore the unknown **mechanism of migration of DNA junctions** (a key complex DNA-restructuring activity) **and other DNA-restructuring activities** of RecQ helicases at the single-molecule level using total internal reflection fluorescence microscopy (TIRFM) (Aim 1), and
- explore how junction migration and resolution complexes enable **DNA repair and proper chromosome segregation in live animals** using 2-photon microscopy (2PM) and confocal microscopy in *C. elegans* animal model system (Aim 2).

Achievements

Below we show representative images and data examples to demonstrate the yet **unpublished achievements** of the project period, and also briefly refer to **published work**.

1. For single-molecule visualization of Holliday junction (HJ) branch migration (a key physical step of HR), during the project we have purchased, set up and optimized the necessary specific (commercial and home-built) components for our **total internal reflection fluorescence microscopic (TIRFM) workstation, combined with an advanced home-built microfluidic manipulation apparatus**.

Microscope optical setup – Figure 1 shows the front view of the TIRF microscope. The opened laser board is shown in **Figure 2**. **Figure 3** shows the optical configuration of the system. This setup, equipped with three laser lines (488, 543 and 642 nm wavelengths), is suitable for single-molecule monitoring of HJ branch migration reactions as described in the project proposal.

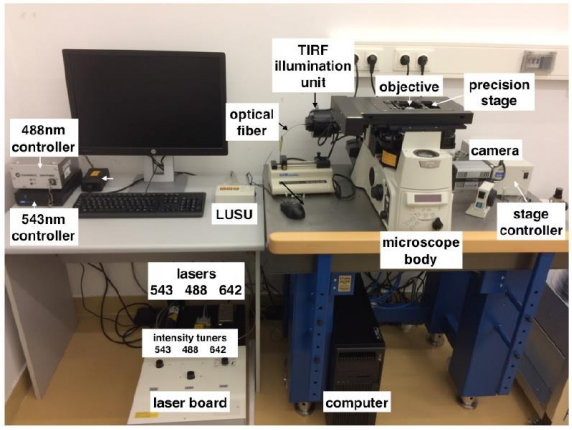

Figure 1: TIRF microscope front view

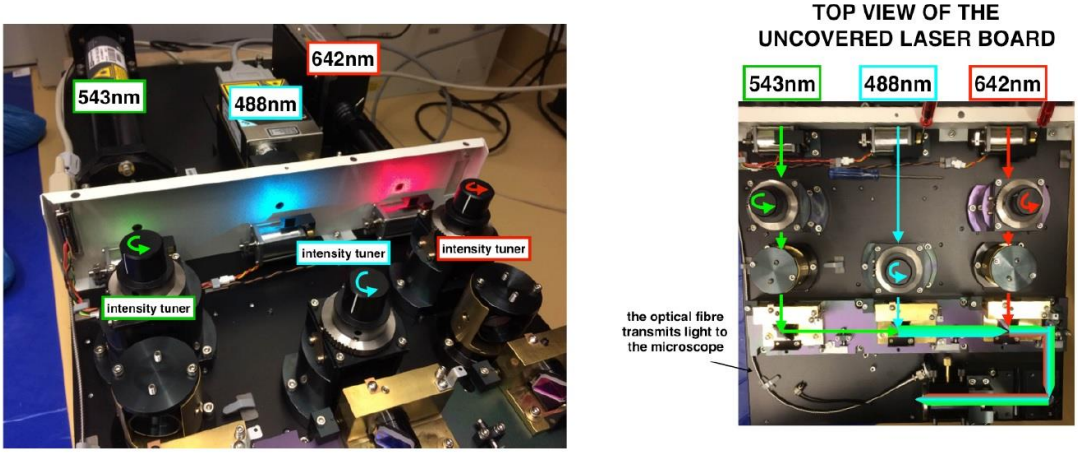

Figure 2: Opened laser board overview

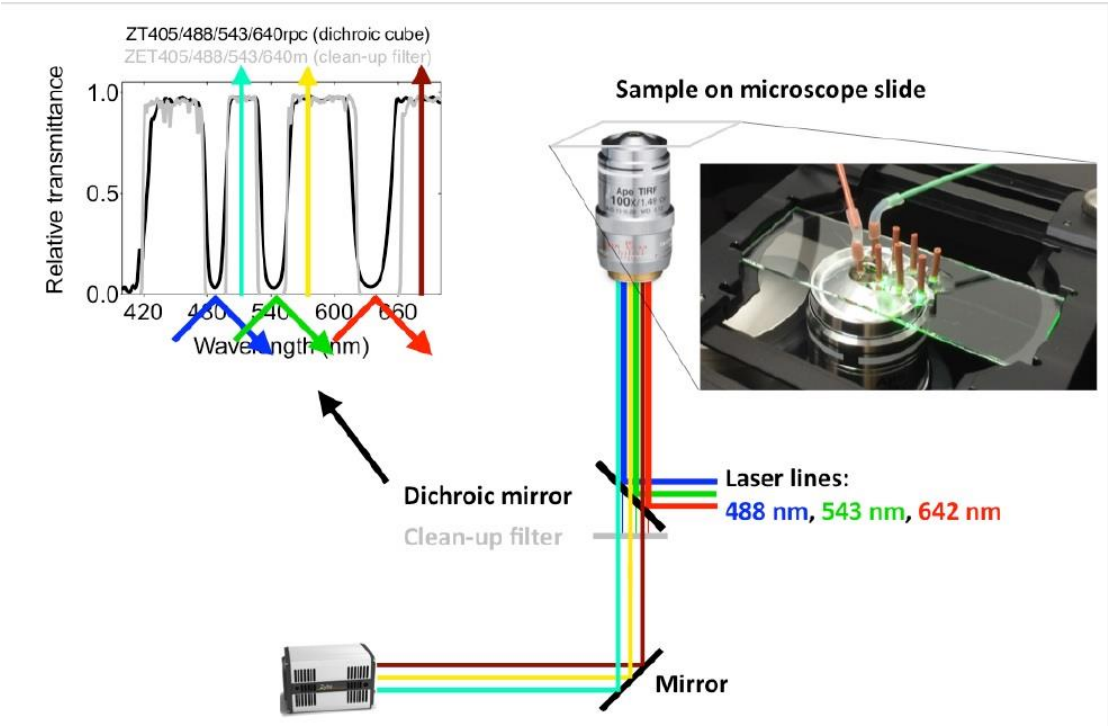

Figure 3: Optical configuration of our TIRFM system

Microfluidic apparatus for DNA immobilization and single-molecule imaging – Figure 4 shows the setup of flow cells that we have designed for single-molecule imaging of DNA molecules and DNA-processing reactions, as described in the project proposal. In this apparatus, three different solutions can be loaded to the flow cell through 'Load 1-3' pathways (**Figure 5**).

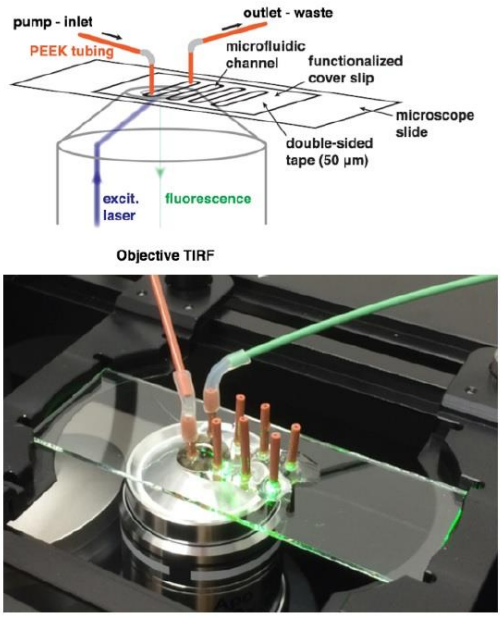

Figure 4: Schematic and real-life design of flow cells

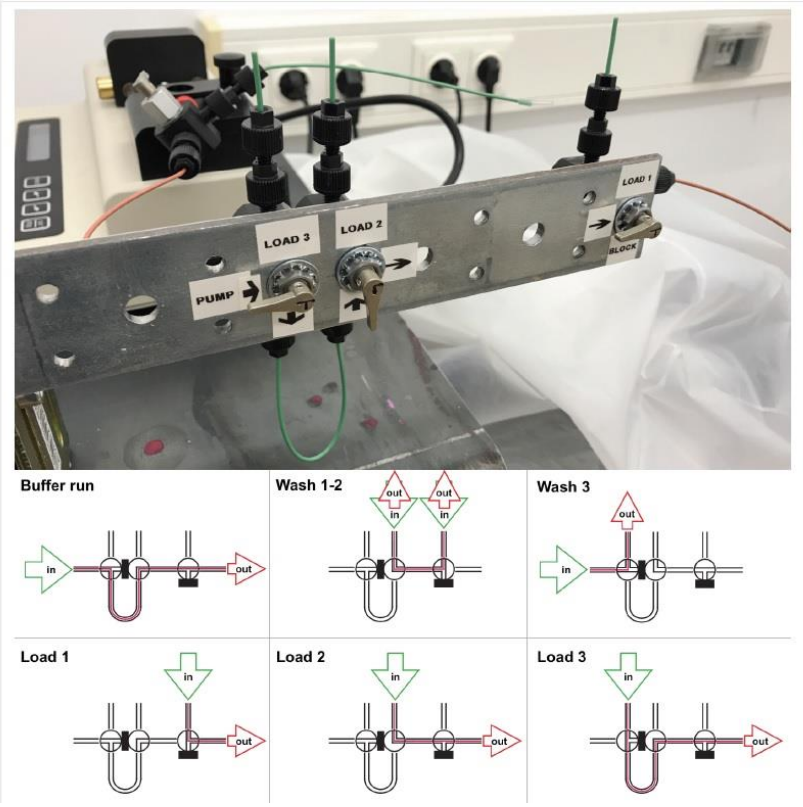

Figure 5: Flow system. The upper image shows the real-life overview of the system. The pump is in the top left corner. The orange PEEK tubing brings the buffer from the syringe to the valve system. The orange tubing on the right side of the mount drives the solutions

directly to the flow cell fixed on top of the objective. The lower image is a schematic representation of the six major flow routes.

2. We have **expressed and purified all protein components** of the BLM-containing dissolvasome (human BLM helicase (purification optimized earlier), topoisomerase III-alpha, RMI1, RMI2; latter three proteins called TRR complex, **Figure 6**). We have also expressed and purified human RPA (Replication Protein A, a single-stranded DNA binding protein), an important interaction partner of BLM (**Figure 7**, see proposal). We measured the ssDNA binding properties of RPA, which closely matched previously published parameters (**Figure 8**).

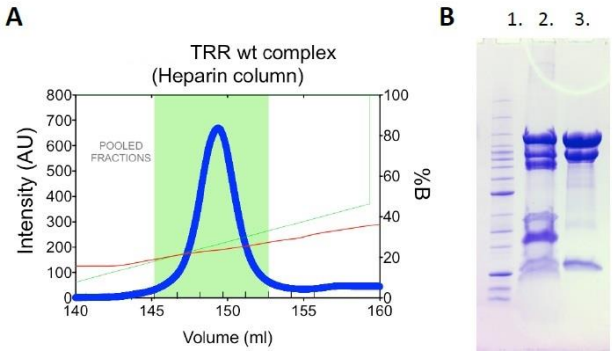

Figure 6: Purification of the TRR complex. (A) Chromatogram of TRR complex elution from a HiTrap Heparin column. Fractions corresponding to the green highlight were pooled. Red line shows conductivity, green line is the percentage of elution buffer. (B) SDS-PAGE analysis. Lane 1: BenchMark ladder, lane 2: Ni-NTA elution, lane 3: final pooled sample after elution from the HiTrap Heparin column (i.e. green shadow in panel A).

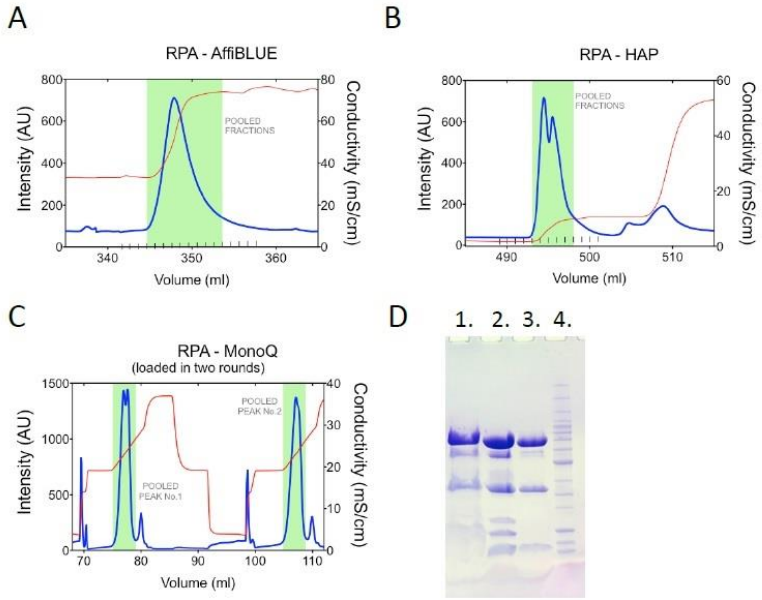

Figure 7: Purification of RPA. (A) Chromatogram of RPA elution from AffiBLUE column. (B) Chromatogram of RPA elution from HAP column. (C) Chromatogram of 2 rounds of RPA elution from MonoQ column. Fractions corresponding to the green highlight were pooled (see panel D). (D) Lane 1: AffiBLUE elution, lane 2: HAP elution, lane 3: final pooled sample after elution from the MonoQ column, lane 4: BenchMark ladder.

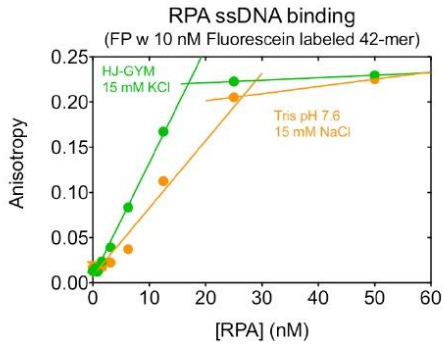

Figure 8: ssDNA binding assay with RPA. Fluorescence anistotropy titrations are shown for a fluorescein-labeled 42mer ssDNA oligonucleotide.

As a functional test, we found that the ATPase activity of ssDNA-bound BLM is affected by RPA but not the TRR complex (**Figure 9**). When the TRR complex was premixed with BLM and RPA was titrated to the mixture, the ATPase activities were practically identical to those in the absence of TRR. This result shows that the TRR complex does not significantly affect the ATPase and RPA interaction properties of BLM.

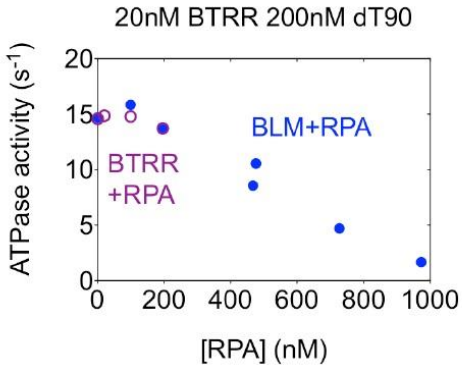

Figure 9: ATPase activity measurements in the presence of BLM (or BTRR complex), dT_{90} (ssDNA) and RPA

3. We have developed and carefully optimized methods to **fluorescently label the BTRR complex**. We have managed to define labeling conditions where the proteins retained their activities, enabling their visualization during enzymatic reactions. We have developed a method to N-terminally label the BLM helicase component of the dissolvasome. Full-length BLM helicase, as well as the monomeric form of BLM (BLM^{1290}; having lower affinity for the protein partners in the complex), were labeled similarly with labeling ratios around 1 fluorophore per monomer and all helicase forms showed only marginally altered biochemical activities after labeling (**Figure 10**). These features enable their use in single molecule assays.

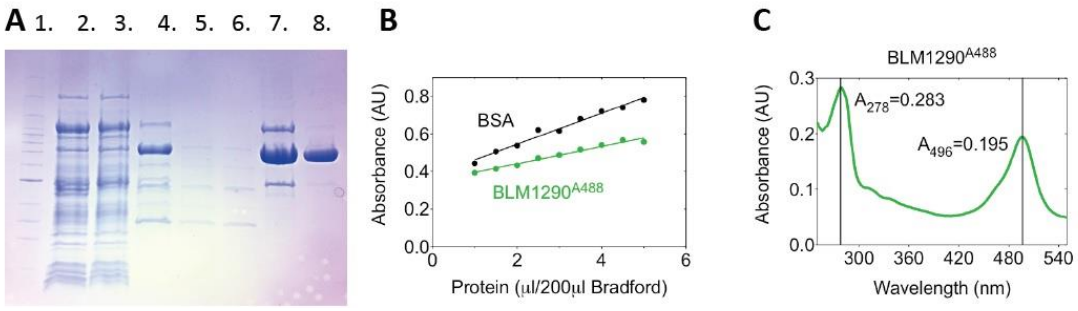

Figure 10: BLM^{1290} purification and labeling with Alexa488. (A) Coomassie stained SDS-PAGE. lane 1: BenchMark, lane 2: supernatant after cell lysis, lane 3: chitin column flow-through, lane 4: chitin column elution, lane 5: heparin column flow-through (at half sample volume), lane 6: heparin column flow-through (at the last few ml), lane 7: heparin column elution, lane 8: final sample (dialyzed after CM column elution). (B) Bradford assay with 0.95 mg/ml BSA. (C) Absorbance spectrum of BLM1290^{Alexa488}.

4. The most challenging part of the project was the **generation of a HJ-containing DNA structure** that can be manipulated and immobilized to the surface of a microfluidic flow chamber placed on the objective of the TIRF microscope. The original concept was to isolate a ~10 kb plasmid and ligate them in a pairwise manner to generate a ~20 kb HJ-arm. This doublet was to be ligated to a (fluorescent) hairpin on one end and to the immobile 'X12' HJ core (annealed from ~50 nt oligonucleotides with appropriate overhangs) on the other end. This structure was planned to be ligated into an *attB* recognition site (for ϕC31 integrase) containing pBlueScript derivative plasmid (pAttB). This HJ containing plasmid (pHJ) was planned to be ligated into λKytos (a lambda phage DNA derivative) to achieve the final λHJ structure (**Figure 11**). We tried to generate the λHJ structure by using the λKytos-PhiC31 integrase system. However, several technical difficulties regarding the ligation of the HJ core and the pre-ligated arms into an *attB* recognition site-containing plasmid hindered the advancement of the project. Thus, we modified the cloning strategy as follows.

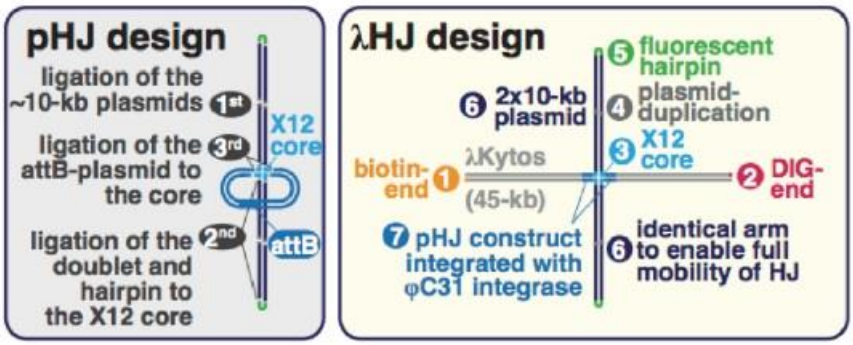

Figure 11: Original design of the λHJ structure

According to the new strategy, the ~10-kb plasmid, pEarlyGate-301, was digested with EcoRI and BamHI. The isolated 9,439 bp fragment was self-ligated and re-digested with EcoRI to generate a plasmid doublet with EcoRI overhangs on both sides. In the middle region, where the two BamHI sites were ligated, the doublet forms a structure that can freely interconvert into a fully mobile HJ (**Figure 12**). This sample was biotinylated and visualized in TIRFM (see below).

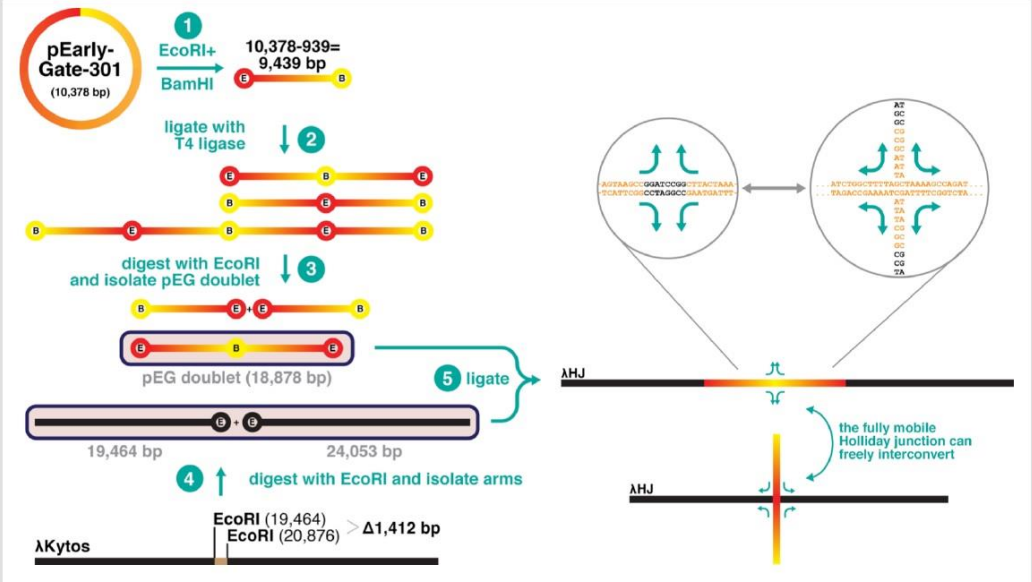

Figure 12: Modified strategy to develop the λHJ structure

5. We have performed **single-molecule characterization of λHJ structure.** Using the above strategy, we were able to visualize the HJ structure in the TIRF microscope (**Figure 13**). The frequency of molecules containing an intensively stained spot (using DNA-binding dyes) in the expected position was in good agreement with the frequency of HJ-containing molecules determined by PCR-based ensemble assays. These results indicate that the intensively labeled spot is indeed the desired HJ structure. These results enable **parallel visualization of the labeled proteins and the HJ structure in the TIRF microscope**.

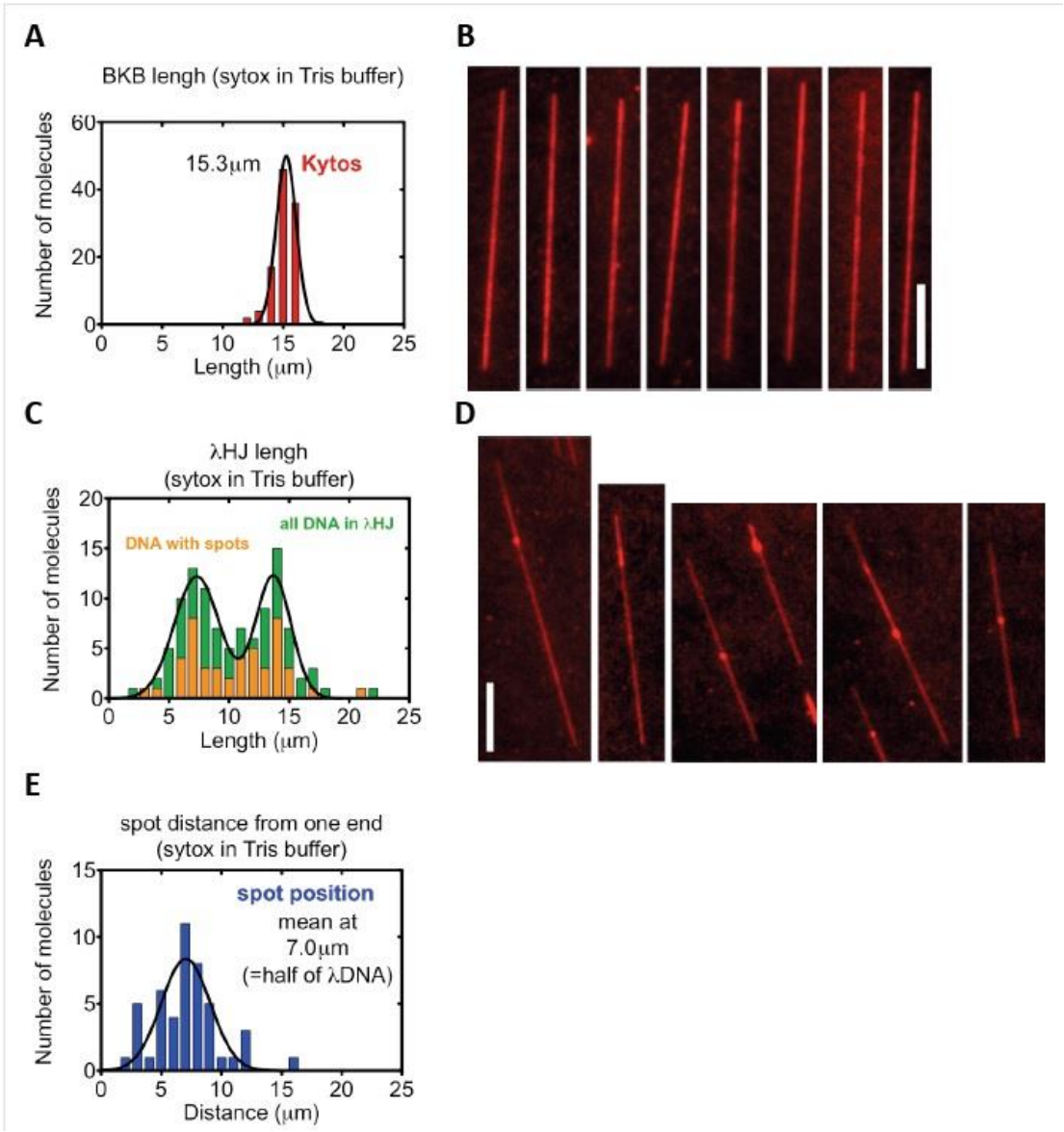

Figure 13: Visualization and length analysis of λKytos (BKB, linear dsDNA) and λHJ (HJ-containing dsDNA) structure. (A) Length distribution of λKytos in Tris buffer. Black line is a Gaussian fit to the histogram. (B) Visualization of λKytos labeled with Sytox Orange. (C) Length distribution of λHJ in Tris buffer. Green bars represent the length distribution of molecules without the intensively labeled spot, orange bars represent the length distribution of the DNA molecules with spots. 47 out of 107 analyzed molecules contained a spot. Black line is a double Gaussian fit to the green histogram. (D) Visualization of λKytos labeled with Sytox Orange. Scale bar is 5 μm. (E) Spot position distribution from one end of the DNA molecules. Black line is the Gaussian fit to the histogram.

6. Although BLM plays central roles in meiotic chromosome segregation, the spatiotemporal distribution of the BLM protein, as well as its interaction pattern with chromosomes and other proteins, is largely unexplored. Meiosis can be readily examined in the germline of *C. elegans*. We have **generated *C. elegans* strains expressing a GFP-labeled variant of HIM-6, the *C. elegans* ortholog of BLM**. We have performed genetic complementation tests and ensured that the HIM-6::GFP protein fully rescues the reduced embryo viability and enhanced male frequency phenotypes characteristic of *him-6* null mutants (**Figure 14**).

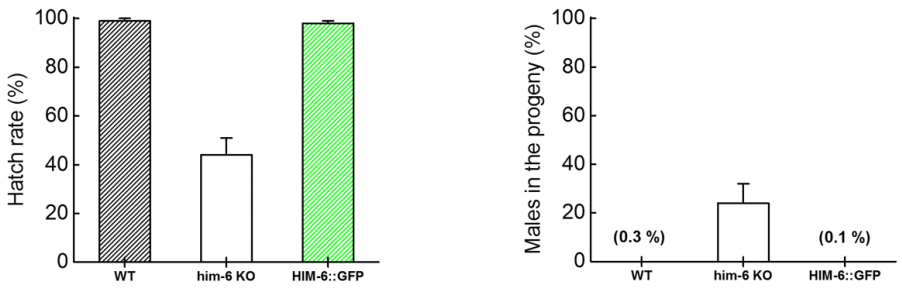

Figure 14: Functional tests on HIM-6::GFP C. elegans

7. We have **successfully introduced a two-photon microscopic (2PM) technology** for the above outlined investigations (**Figure 15**). Furthermore, we have generated a *C. elegans* strain co-expressing **mCherry-labeled histone and HIM-6::GFP proteins**, thereby solving the problem of simultaneous detection of chromosomes and the HIM-6 protein in live animals. These developments enabled us to determine with high precision the previously unknown spatiotemporal distribution of HIM-6 during different stages of germline development (**Figure 16**). Based on observed chromosome structure, we divided the *C. elegans* gonad to seven different zones corresponding to meiotic phases as cells pass from the mitotic zone eventually to developed oocytes (**Figure 15-16**).

We found that HIM-6 is not expressed in the initial (mitotic) zone. Its first appearance was observed in the short transition zone and, thereafter, we found a burst of HIM-6 expression in the early and middle pachytene zones (**Figure 15-16**). In late pachytene, the presence of HIM-6 suddenly decreases and is retained around one focus per chromosome. This tendency is observed through diakinesis. In oocytes, HIM-6 entirely disappears.

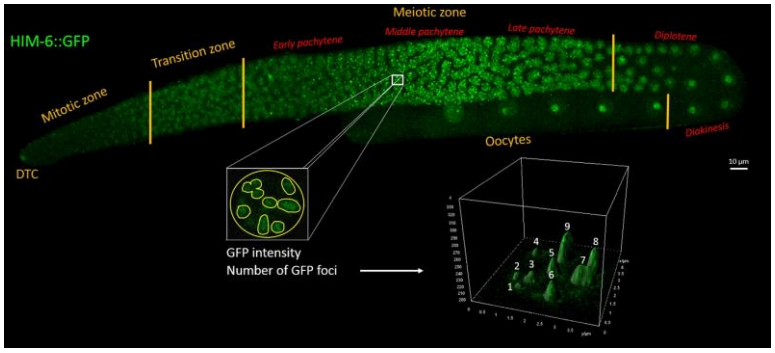

Figure 15: 2-photon microscopic imaging of HIM-6::GFP *C. elegans* gonad

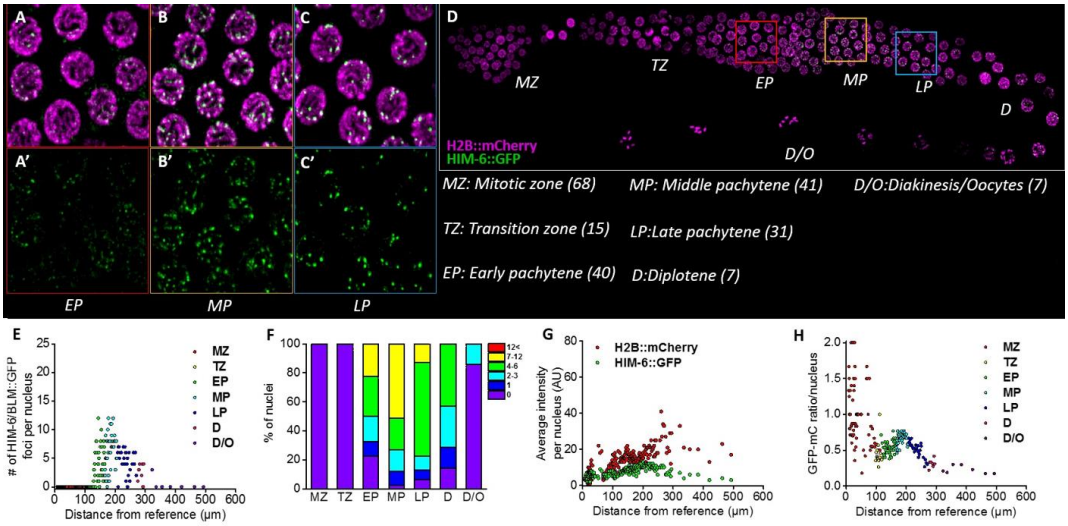

Figure 16: Observation of the dynamics of chromosome-associated HIM-6::GFP foci during *C. elegans* germ line development

8. The rapidly increasing appearance pattern of HIM-6 in pachytene overlaps with that of RAD-51 recombinase, a key early HR protein component. In later phases including late pachytene and diplotene, the HIM-6 appearance pattern follows that of COSA-1 (a key player in in crossover site designation and licensing). We have performed RNAi knockdown experiments targeting key HR components, and these experiments **revealed functional interactions between HIM-6 and the assessed HR proteins** (**Figure 17**).

Our findings revealed that **HIM-6 plays key roles both in the initial and late phases of meiotic HR**. During early HR, HIM-6 assists in eliminating redundant joint DNA molecules, whereas in later phases it assists in the resolution of HJ structures and licensing these for crossovers (CO) in order to support proper chromosome segregation (**Figure 18**).

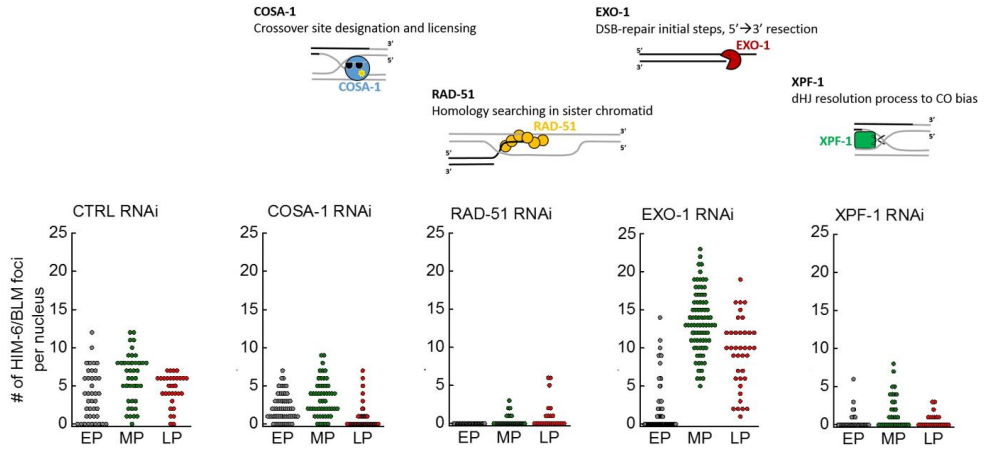

Figure 17: Determination of the effect of functional interactions of HIM-6 with key HR factors. EP, early pachytene; MP, middle pachytene; LP, late pachytene.

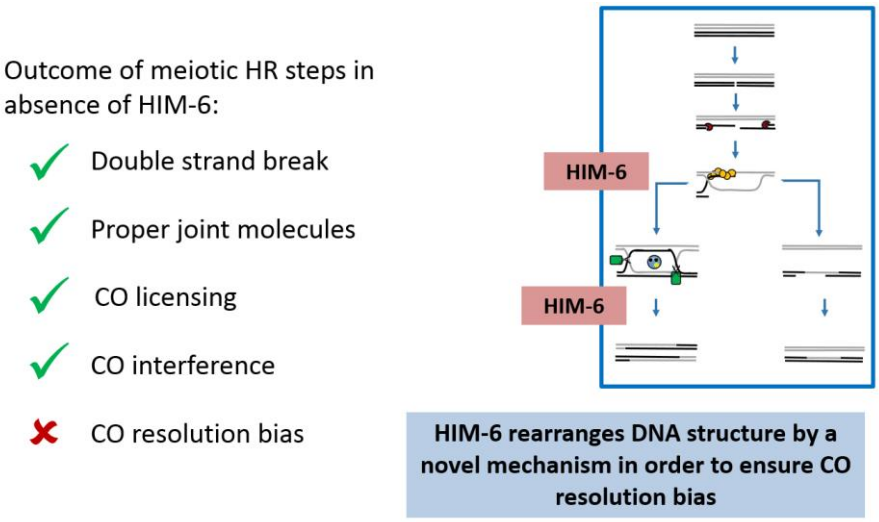

Figure 18: Emerging novel roles of HIM-6 in precise HR and faithful chromosome segregation during meiosis

9. Besides the above achievements, in the project period we have published the discovery of a novel HR quality control mechanism based on RecQ helicase activities (ref. 1), we have used the developed enzyme kinetic techniques for the elucidation of the mechanism of action of an important metabolic enzyme (2), we have revealed a biophysical mechanism whereby RecQ helicase gains access to its DNA substrate via a specific protein-protein interaction (3), we have revealed the functional linkage between HR initiation and quality control systems (4), and defined the DNA-binding mechanism of human RAD51 recombinase, a key interacting partner of BLM helicase (5).

Perspectives and strategy

1. We are in the process of analyzing the HJ migration mechanism of the BTRR complex, as well as processing the data on the functional roles of HIM-6 in germ line development. We have started the preparation of publications in both topics. Given that these areas have not been previously explored and our data reveal novel, crucial mechanistic information **both on the physical mechanism (Aim 1) and the *in vivo* outcome (Aim 2) of the DNA-restructuring activities of the BLM helicase**, we expect to publish these results in leading, high-impact journals of the field.
2. The above mentioned results, together with the results already published before and during the project period, will serve as a basis for preparing a **competitive ERC Grant application** in the next application round (scheduled to be submitted in August 2018).

References

**: equal contributions*

1. Harami, G. M., Seol, Y., In, J., Ferencziová, V., Martina, M., Gyimesi, M., Sarlós, K., Kovács, Z., J., Nagy, N. T., Sun, Y., Vellai, T., Neuman, K. C.*, **Kovács, M.*** (2017): Shuttling along DNA and directed processing of D-loops by RecQ helicase support quality control of homologous recombination. *Proc Natl Acad Sci USA 114:* E466-E475.
2. Horváth, G., Biczók, L., Majer, Z., **Kovács, M.,** Micsonai, A., Kardos, J., Toke, O. (2017): Structural insight into a partially unfolded state preceding aggregation in an intracellular lipid-binding protein. *FEBS J. 284:* 3637-3661.

3. Mills, M., Harami, G. M., Seol, Y., Gyimesi, M., Martina, M., Kovács, Z. J., **Kovács, M.*,** Neuman, K. C.* (2017): RecQ helicase triggers a binding mode change in the SSB-DNA complex to efficiently initiate DNA unwinding. *Nucleic Acids Research 45:* 11878-11890.
4. Ferencziová, V., Harami, G. M., Németh, J. B., Vellai, T., **Kovács, M.** (2018): Functional fine-tuning between bacterial DNA recombination initiation and quality control systems. *PLoS One.* 2018 Feb 22;13(2):e0192483.
5. Špírek, M., Mlčoušková, J., Beláň, O., Gyimesi, M., Harami, G. M., Molnár, E., Novacek, J., **Kovács, M.*,** Krejci, L.* (2018): Human RAD51 rapidly forms intrinsically dynamic nucleoprotein filaments modulated by nucleotide binding state. *Nucleic Acids Research* 2018 Feb 22. doi: 10.1093/nar/gky111.